Large-eddy simulation of turbulent cavitating flow in a Diesel injector including needle movement, in OpenFOAM®

Konstantinos Kolovos*[1], Nikolaos Kyriazis[2], Phoevos Koukouvinis[2]
Manolis Gavaises[2], Jason Z. Li[3], Robert M. McDavid[3]
[1]Perkins Engines Company Ltd, Peterborough, PE1 5NA, United Kingdom
[2]City University London, Northampton Square EC1V 0HB, United Kingdom
[3]Caterpillar Inc, Mossville, IL 61552, United States
*Corresponding author: Konstantinos.kolovos.2@city.ac.uk

Abstract

In this work the turbulent cavitating flow, inside a five-hole common rail Diesel injector and the effect of cavitation on erosion is investigated for the opening cycle of the injection. An explicit density-based solver of the compressible Navier-Stokes (NS) equations of the Arbitrary Lagrangian–Eulerian (ALE) formulation, suitable for cavitating flows is implemented in the open-source CFD code OpenFOAM®. Numerical fluxes are calculated based on the hybrid approximate Riemann solver. The hybrid scheme provides a Mach number consistent numerical flux, suitable for subsonic up to supersonic flow conditions. Finite Volume (FV) discretization is employed in conjunction with a fourth order Runge-Kutta time integration scheme. The thermodynamic closure is based on a barotropic Equation of State (EoS) for the liquid and vapour phases. The cavitation model is based on a thermodynamic equilibrium assumption and the compressibilities of the liquid and the liquid-vapor mixture are taken into account. The injector needle movement is represented by a cell-based mesh deformation method to ensure mass conservation which accounts for the Space Conservation Law (SCL). This work focuses on potential erosion and on the development vortical structures. First, the potential erosion regions are predicted though three different indexes, the maximum collapse pressures and the erosion damage model. The latter is coupled with the CFD code. The three indexes are compared with experimental results, from CT scans. The structure of the flow is analysed with an emphasis on the interaction between coherent vortical structures and cavitation. The Wall Adapting Local Eddy viscosity (WALE) LES model was used to predict incipient and developed cavitation, while also capturing the shear layer instability, vortex shedding and cavitating vortex formation. The analysis of the turbulent flow field reveals that the opening phase of the injection event consists of four different stages. Initially a negative mass flow rate is observed, followed by a second stage characterized by a complex vortical cavitation in the sac. String cavitation in the orifice is observed during the third stage. At the last stage the cavitation region in the orifice exhibits coherent cavitation structures both in the axial line as sting cavitation and on the orifice surface as shear induced cavitation. Violent collapse events of cavitation structures are detected during the opening phase. Moreover, this work revealed the formation of thin and thick string cavitation in the orifice volume and the effects on the flow pattern in the orifice and at the exit of the orifice.

Keywords

ALE, explicit density - based compressible solver, two-phase model, erosion pattern, OpenFOAM®, LES, vortex - string cavitation

Introduction

The characteristic fuel nozzle size for diesel injectors is of the order of several hundred micrometres. This geometric scale makes experimental flow characterization within an injector challenging. Experimental assessment of erosion damage can supply information about regions of high structural stresses, which can be linked to the occurrence of cavitation, but it does not provide insight to all the aspects of the underlying flow dynamics needed for the optimization, of the performance of the injector. Computational fluid dynamics, though can provide time-resolved information on flow structures in arbitrary small geometries. Thus, detailed numerical simulation of cavitating flows has become an increasingly important tool in the design process of injection systems.

The numerical work by Örley et al. [1] on Diesel injectors involves the immersed boundary method, needle motion, compressibility of liquid, vapour and free gas, though the focus is mainly on the developed turbulent structures. Further examples in the literature discuss cavitating duct flows and single hole injectors, five-hole injectors, and six-hole injectors with no explicit comparison of the erosion patterns to an experiment, (Befrui et al. [2] and Duke et al. [3]) . Moreover, Koukouvinis et al. [4], assessed the impact of the large vortical structures within the nozzle flow and the interaction with incipient and developed cavitation in multi-phase flows and highlighting the need for Large-Eddy Simulations (LES). There have been several efforts to predict cavitation in Diesel injectors, (Gavaises et al. [5] and Koukouvinis et al. [6]). The aim of the work by Koukouvinis was to simulate the flow inside a Diesel injector in a more fundamental level by focusing on pressure peak/erosion development, including needle motion, compressibility effects turbulence and transient effects incorporating the transient effects of the needle motion within the LES framework.

The aim of this research is to assess the impact of turbulence and cavitation in a diesel injector flow involving a moving computational domain. The injector needle movement is represented by a cell-based mesh deformation method. To ensure the mass conservation the mesh fluxes are evaluated in the discretized equations as described by the ALE approach, as proposed by Perić et al. [7] guaranteeing enforcement of the Space

Conservation Law (SCL) [7]. Diesel injector design is evaluated, starting at an initial needle lift of 0.6 µm and continuing until 295 µm. To capture the complex flow field and cavitation structures forming in the Diesel injector the WALE viscosity model combined with an explicit density-based solver of the compressible NS equations using barotropic EoS (Egerer et al. [8]) has been implemented. The aim of the study was also to detect the regions of the collapse of cavitation structures, which is directly linked with the formation of extreme local pressure and therefore erosion damage. The simulation results, specifically the extreme local pressure and the simulated damage erosion show a good correlation with the X-ray scans of the experimental injectors.

The WALE LES model, [9] was able to predict incipient and developed cavitation, while capturing the shear layer instability, vortex shedding and cavitating vortex formation. The analysis of the turbulent flow field reveals that the opening phase characterized by four different stages. Validation of the numerical method is performed using the erosion model proposed by Dular et al. [10], which is based on the physical description of phenomena from cavitation cloud implosion and pressure waves and of pit formation depth. The coupling between CFD and the erosion model is based on the use of the mechanical properties of hardened AISI 52100 steel, [11]. LES with the employed cavitation erosion modeling predicts relevant flow and cavitation aggressiveness features accurately. The turbulence structure of the flow is further analysed with an emphasis on the cavitation and vortex interaction and on the mass flow rate. This paper is structured as follows. First, the mathematical and physical model is presented. Then, the numerical approach is analysed. Description of the Diesel injector geometry, erosion pattern and the computational setup are provided. In the fourth section the flow-field during the different stages of the full injection opening cycle with respect to cavitation and vapor collapse characteristics are presented. In the fifth section the results from the computational analysis is compared with the erosion pattern retrieved from experiments. Finally, the effects of fluid flow turbulence are presented.

Mathematical and physical model

The solver described in this chapter is based on the explicit density based solver on the OpenFOAM® version 2.4.x [12], which is called rhoCentralFoam [13]. RhoCentralFoam is a single-phase solver using the Tadmor-Kurganov numerical flux [14] and the ideal gas assumption. The EoS and the space discretization which described below have been implemented on the modified solver aiming to model two or three phases. The flow field is modelled by the barotropic modelling approach. The integral formation for the mass and momentum transport for a moving mesh, within the ALE framework [7], is solved. In the described formulation of the NS equations the volumetric conservation is implemented by the Space Conservation Law (SCL) and are expressed as:

$$\frac{\partial}{\partial t}\int \rho dV = -\oint \rho \left(\vec{U} - \vec{U_b}\right)\cdot \vec{n}dS, \tag{1}$$

$$\frac{\partial}{\partial t}\int \rho \vec{U}dV = -\oint \rho \left(\vec{U} \otimes \left(\vec{U} - \vec{U_b}\right)\right)\cdot \vec{n}dS + \oint \tau \cdot \vec{n}dS - \oint p \vec{n}dS + \int \rho \vec{g}dV, \tag{2}$$

$$\frac{\partial}{\partial t}\int dV - \oint \vec{U_b}\cdot \vec{n}dS = 0. \tag{3}$$

The relationship between the rate of change of the volume V of a computational cell and the velocity of the boundary surface is defined by the SCL. To ensure mass conservation, the space conservation law [15], is enforced. The discretization of the above equations [1-3] depends on the temporal integration scheme and it allows for the calculation of the mesh motion flux Φ_{fmesh} on the basis of the swept volume $\dot{V}_b$. In the simple case of Euler integration, the mesh motion flux can be calculated as:

$$\Phi_{fmesh} = \left(\vec{U_b}\cdot \vec{n}\right)_f dS = \dot{V}_f \tag{4}$$

Space discretization

In cavitating flows there is large variation in the speed of sound and the Mach number, making the approximation of the interface fluxes challenging. The flow can be considered incompressible in the liquid regime and the Mach number can even be of the order of 10^{-2}. On the other hand, in the vapour regime and during the collapse of the cavity structures where shock waves are created, the flow is highly compressible and the Mach number can be of the order of 10^2 or even higher. When using density-based solvers for low Mach number flows, slow convergence and inaccuracies in the solutions have been noticed [16]. To overcome this, the Mach consistent numerical flux of Schmidt et al. [17], validated by Kyriazis et al.[18] for the investigation of bubble dynamics, has been implemented. This scheme is based on the HLLC and AUSM flux, Meng-Sing [19]. The advancement of a four stage Runge - Kutta (RK) method, fourth order in time has been implemented. The allowable step size is usually determined based on the following three factors, absolute stability (linear stability), robustness (nonlinear stability) and accuracy as described in Toro [20].

$$u_f = \frac{1}{\rho_L + \rho_R}\left(\rho_L u_L + \rho_R u_R + \frac{p_L - p_R}{c_f}\right), \qquad p_f = \frac{p_L + p_R}{2}, \qquad c_f = max(c_L, c_R). \tag{5}$$

Two phase cavitation model for Diesel Fuel B0 2015

Since Diesel properties vary significantly with the pressure levels in the injection systems, both liquid phase viscosity and density are assumed to vary with pressure only. A two-step barotropic equation of state is used by Koukouvinis et al. [6]. The modified Tait equation of state is used for the liquid phase. For the vapour mixture the

isentropic approximation proposed by Egerer et al.[8]is used. The piece -wise EoS is provided by the following expression for the pressure as a function of density:

$$p(\rho) = \begin{cases} (B + p_{sat})\left[\left(\dfrac{\rho}{\rho_{sat,L}}\right)^n\right] - B, & \rho \geq \rho_{sat,L} \\[2ex] p_{sat} + C_1\left[\dfrac{1}{\rho_{sat,L}} - \dfrac{1}{\rho}\right], & \rho < \rho_{sat,L} , \end{cases} \tag{6}$$

with C_1 and n liquid dependent constants and $\rho_{sat.L}$ is the density at saturation pressure p_{sat}. This equation of state has the advantage that can handle both large and negative absolute pressures. For all materials the exponent n is set to 7.15, since such values correspond to weakly compressible materials such as liquids. For the injector flow the properties of the liquid are considered on an average temperature level of 396 K. B is fluid-specific parameter, c is speed of sound and the vapour fraction is a function of density, as shown in (7). A specific reference state, following Safarov et al. [21], is chosen. In Table 1 and 2, the numerical values for the reference state for computing the Tait parameters are provided. The saturation point properties for the liquid and the vapour phase are provided in Table 3. Also, the liquid and vapour phase in the cavitating liquid is assumed to be in thermal and mechanical equilibrium and we apply the homogenous-mixture cavitation model.

$$B = \frac{\rho C_1^{\;2}}{n}, \qquad\qquad\qquad c = \sqrt{\left(\frac{\partial p}{\partial \rho}\right)_S}, \tag{7}$$

Property	unit	value
Inlet pressure	[10^6 Pa]	180
Density	[kg/m^3]	851
Speed of sound	[m/s]	1700

Table 1. Thermophysical properties at 180 MPa, 396K.

Property	unit	value
Outlet pressure	[10^6 Pa]	5
Density	[kg/m^3]	750
Speed of sound	[m/s]	1070

Table 2. Thermophysical properties at 5 MPa, 396K.
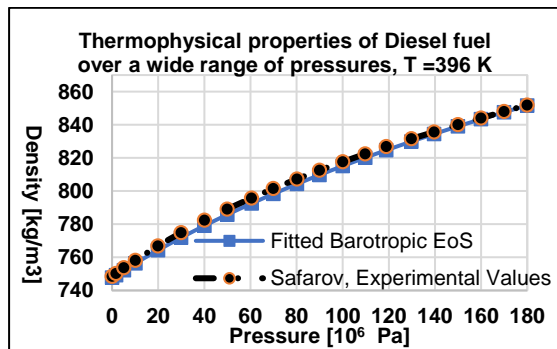
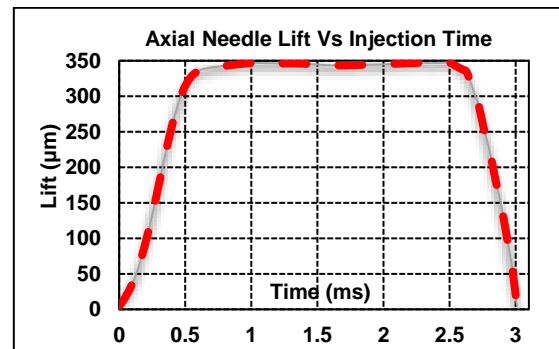**Figure 1.** EoS with reference data of Safarov et al. [21]

Figure 2. Needle motion of the injector.

Property	unit	value
Saturation pressure	[Pa]	8000
Saturation density, L	[kg/m^3]	747
Speed of sound	[m/s]	1060
Saturation density, V	[kg/m^3]	0.1
Viscosity, L	[Pa s]	0.0006
Viscosity, V	[Pa s]	7.49* 10^{-6}

Table 3. Fluid parameters for isothermal Diesel B0 2015.

	unit	value
Needle radius	mm	1.711
Orifice length	mm	1.262
Orifice diameter	mm	0.37
Entrance Din Orifice diameter	mm	0.359
Exit Dout Sac volume	mm^3	1.19
K-factor Din -Dout	-	1.1

Table 4. Geometric dimensions of the examined injector.

Description of the examined injector and testing conditions

The validation of the new solver is presented for the case of an unsteady simulation for Diesel fuel within a moving injector needle with dynamic mesh deformation. The geometry is represented in Figure 3 and the details of the injector geometry are presented in Table 4. The simulation was carried out using the WALE model that is designed to return the correct wall-asymptotic behaviour for bounded flows. This efficient SGS model is proposed by Nicoud and Ducros (1999) [9], which is based on the square of the gradient tensor and is characterised by a realistic near wall behaviour. The spatial operator consists of a mixing of both the local strain, rotation rates and the eddy viscosity goes naturally to zero in the vicinity of a wall. As shown in Figure 4 the injector consists of five orifices, but only the 1/5th of the domain was simulated. Symmetry boundary conditions have been applied at the side of the computational domain. The needle motion is assumed to be in the axial – z direction only and no eccentricity effects were considered. The total injection duration is 3 ms as shown in Figure 2. Pressure boundary conditions are set according to the upstream pressure profile and downstream pressure, while needle motion is set according to the needle lift profile, shown in Figure 2.
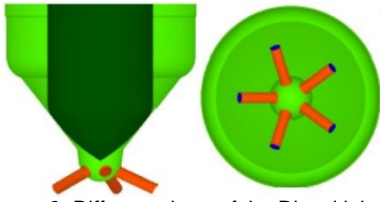
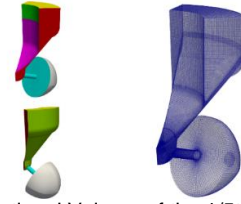**Figure 3.** Different views of the Diesel injector.

Figure 4. Computational Volume of the 1/5th of injector.

The computational mesh used consists of a hexahedral block structured zone, with the exception of an unstructured tetrahedral zone in the sac volume before the orifice entrance. Mesh motion is performed with a cell-based deformation algorithm which moves the computational points and cells and it stretches the cells in a uniform way. The needle lift was initially set at 0.6 μm with 5 cells in the gap between needle and needle seat. The initial field was obtained from a steady state run. Significant turbulence is expected to be generated, as will be shown later, during the lift of the needle between the needle seat passage, inside the sac volume and in the orifice. The total cell count of the computational mesh is initially almost 1.0 million computational cells and finally reaches a peak of 1.8 million cells. A pure linear second order scheme was used for the interpolation of the flow field variables, while a hybrid scheme between central and second order upwind was used for the reconstruction of the conservative variables. The erosion patterns from the endurance tests are shown in Figure 5. The Figure shows the X-ray CT scans of the sac/orifice and needle of two prototype Diesel injectors with the same endurance test hours.
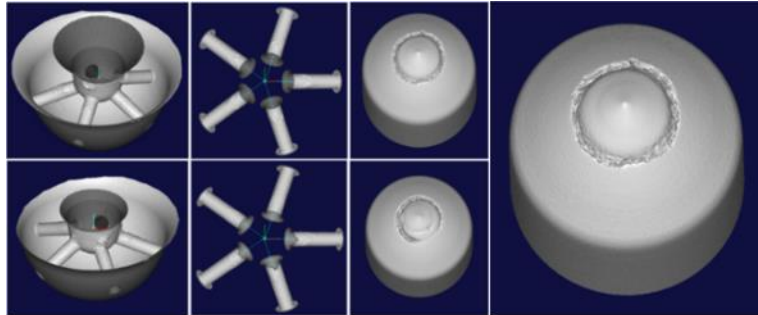

Figure 5. From left to right. Erosion details at various locations, as found on the surfaces of two examined injectors of the same design after the same operation hour. Analysis of the needle surface erosion pattern using image processing tool.

In Figure 5, the analysis of the erosion pattern of the needle surface is presented. By using two different methods the inner and the outer radii of the erosion ring pattern is identified. These radii were found to be 0.6 mm and 0.8 mm. The experimental results obtained from all the endurance tests suggest that the erosion patterns are consistent, that is a similar erosion trend develops for injectors tested, at the same time intervals. This injector has signs of erosion damage inside the sac volume that become apparent rather later, after thousands of hours of continuous operation. The sac volume seems to be much less affected by erosion damage than the needle while the injector holes are barely affected by erosion. In the nozzle holes, the injector is generally less prone to erosion damage, where the damage is minor, in the form of a minor pit near the orifice entrance.

Analysis of the flow field

The analysis of the turbulent flow field reveals that the opening phase consists of four different stages.
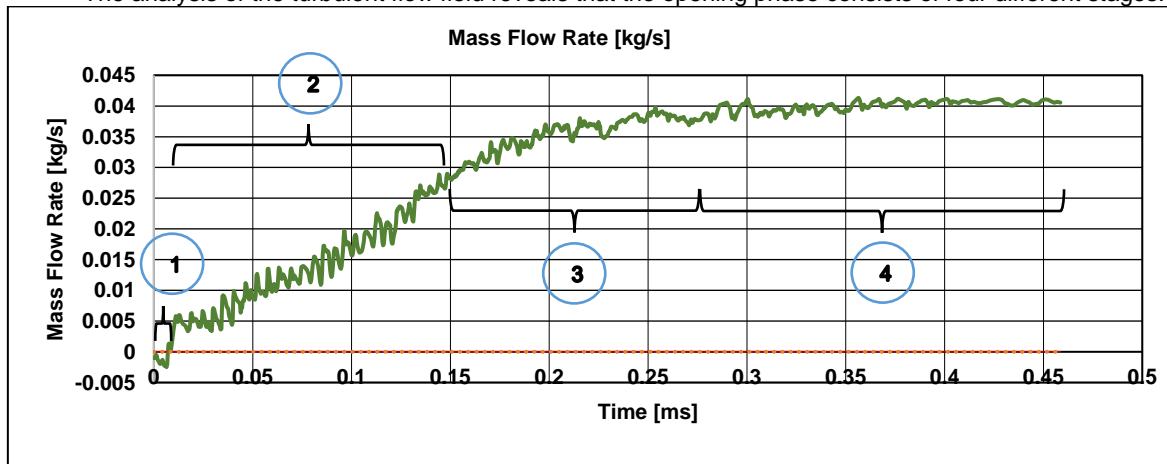

Figure 6. Temporal evolution of the mass flow rate. During the opening phase, the flow filed inside the injector characterized by four different stages which influence significantly the erosion pattern and the cavitation vortex and cavitation string structures in the injector.
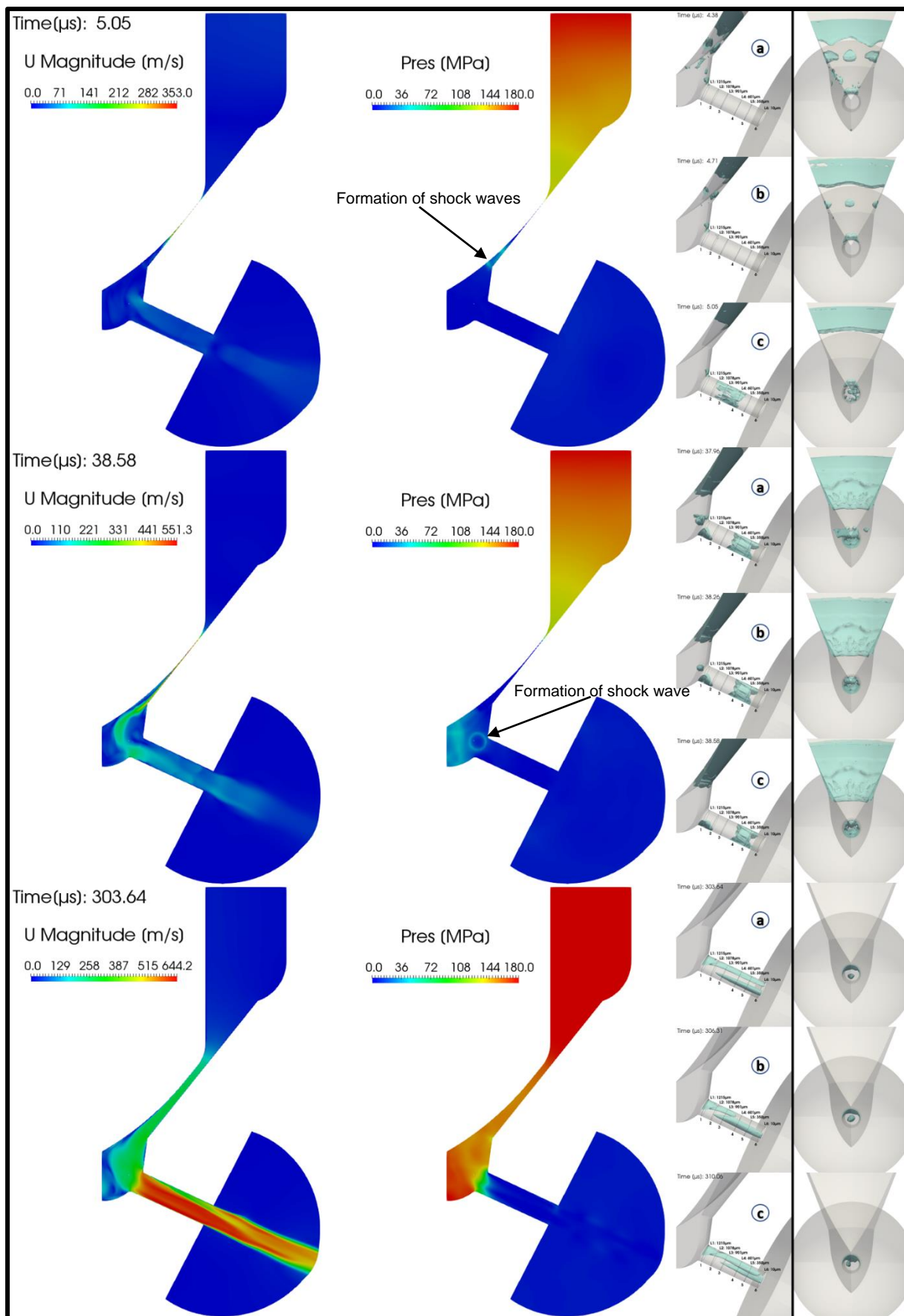
Figure 7. Top to bottom: Realisation of the flow field inside the Diesel injector for three instances (T=1 T=2 T=3). Left column: Velocity magnitude distribution at the midplane. Center column: Pressure distribution. Right: Vapour distribution at three different instances (a-c). A series of images (a-c) illustrating the growth, developed and the collapse of the developed cavitation formation.

During the stage 1, (see Figure 6), between 0.06 µs and 6 µs, a negative mass flow rate is observed. As seen in Figure 7(Right), at injection time 5.05 µs the shear layer instabilities in the needle seat passage triggers the formation of dense attached cavitation. The external front part of the cavitation formation is separated and it collapses before the entrance in the sac volume, as illustrated in Figure 7(Right), (c). As shown in Figure 7(Center), at injection time 5.05 µs strong collapse events of vapor structures in the needle seat cause the formation of shock waves.

During the stage 2 of the opening phase, (see Figure 6 from 6 µs up to 150 µs), complex cavitation appears both at the needle seat, at the sac and in the orifice, as shown in Figure 7(Right), (a-c), at injection time 38.58 µs. The attached cavitation at the needle is more extended and protrudes into the sac. This vapour distribution interacts with the flow in the sac inducing vortices that result in further cavitation in the orifice. As observed from the three consecutive realisations around the instance 38.58 µs a vortex cavitation formation appears within the sac (a) and (b) collapses at time (c) resulting in a shock apparent in the pressure distribution, as shown in Figure 7(Center). A sheet cavity formation is observed at the perimeter of the orifice and limits the mass flow rate.

During the stage 3 of the opening phase, (see Figure 6 from 150 µs up to 270 µs), a transition of the cavitation from the lower to upper orifice surface is predicted. Unstable vortex string formations initiates from the orifice inlet and significantly influence the formation the velocity field even after the orifices exit. As shown in Figure 6 the stage 4 of the opening phase, (see Figure 6 from 270 µs up to 470 µs), cavitation occurs only in the orifice volume, as shown in Figure 7(Right), (a-c), at injection time 303.64 µs. The flow is attached at the vertical wall of sac volume, as seen in Figure 7(Left). As illustrated in Figure 7(Right), (a-c), sheet cavitation formation is observed at the upper orifice surface and large stable vortical and vapor structures in the axial direction now dominate the flow. Due to the tapered shape of the nozzle holes, these vortices are further stretched and cause vortex cavitation at the nozzle outlet plane. The visualizations of the vapor shedding cycle shown in Figure 7(Right), (a-c).

Comparison with experimental data: Cavitation Erosion

From the experiments a clear pattern is identified with erosion formation on the needle surface in the form of a deeply engraved ring shape, more specifically a ring with inner and outer radii of 0.6 mm and 0.8 mm (Figure. 5). Considering the sac damage, the injector needle is less affected by erosion very close to orifice inlet.
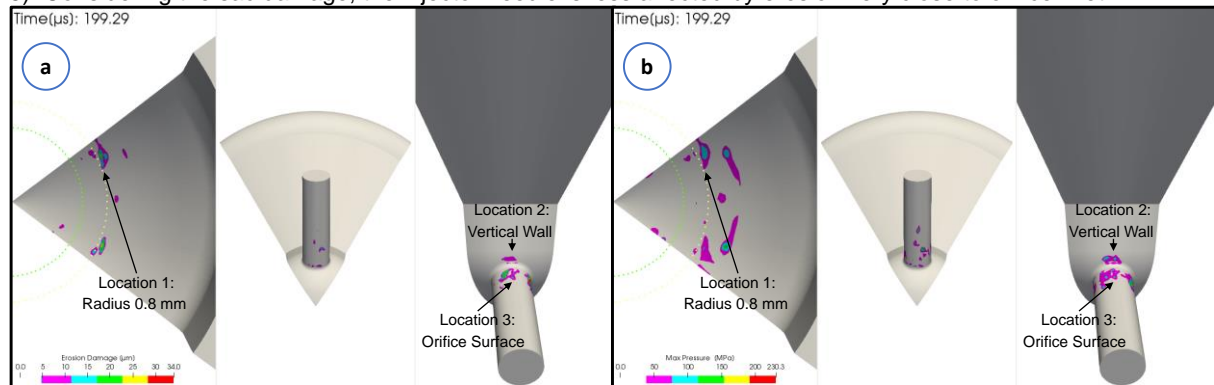

Figure 8. Spatial distribution of potential cavitation damage. (a) Erosion damage prediction [µm]. (b). (B) Maximum wall collapse pressures recorded at the walls [MPa].

A pit-count method proposed by Dular et al. [10], was applied to evaluate the potential damage. The erosion model is based on the physical description of phenomena from cavitation cloud implosion, pressure wave emission and its attenuation, micro-jet formation and finally to the pit formation.

As shown in Figure 8, the three locations with potential erosion are predicted very well from the simulation results. These locations are at the orifice inlet, at the sac vertical wall and on the needle surface. The identification of erosion sensitive areas during the design process of fuel injectors is a key factor for performance optimization and durability. The erosion prediction from pressure peaks, in Figure 8(b), significantly exceeding and shows a very good agreement with the experimental data, at all the investigated regions, including needle, vertical sac wall and orifice inlet. All of these methods-indexes could potentially correlate to the erosion patterns. In order to detects isolated vapor-structure collapses (collapse detector) a collapse detector algorithm is used for all the mentioned indexes. In order to compare the numerical results with the experimental data two circles are used positioned at radius 0.6 mm and 0.8 mm. In the Figure. 8(a) the potential erosion damage until injection time 199.29 µs is presented. In Figure. 8(a) the potential damage is predicted at almost at the same locations of the injector geometry. After injection time 150 µs no more cavitation formation is predicted in the needle seat passage region. The predicted results from the erosion damage model are in very good agreement with the experimental data. Moreover, the maximum collapse pressure field and the erosion damage model have a good correlation with the erosion pattern from the experimental data, specifically at the needle surface, at the upper orifice surface and on the vertical wall of the sac volume, but both of these indexes predict a small pit formation at the lower orifice surface.

Interaction between vortical structures and cavitation mechanisms

Figure 9 shows the prevalent streamwise vortical structures, in different cross-sections. At needle lift 63.7 µm and injection time 154.31 µs, a small separation which is visible on the lower side of the orifice near the inlet edge disappears before the second cross section, as shown in Figure 9, **(**cross-sections 1 and 2). This vortical structure originates from the boundary-layer separation of the flow in the sac region. Its size increases significantly to 95% of the orifice length, see Figure 9 (cross-sections 1-6, and image c, at injection time 155.73 µs). Due to the acceleration of the flow, the resulting streamwise velocity gradient stretches this cavity forming string cavitation.
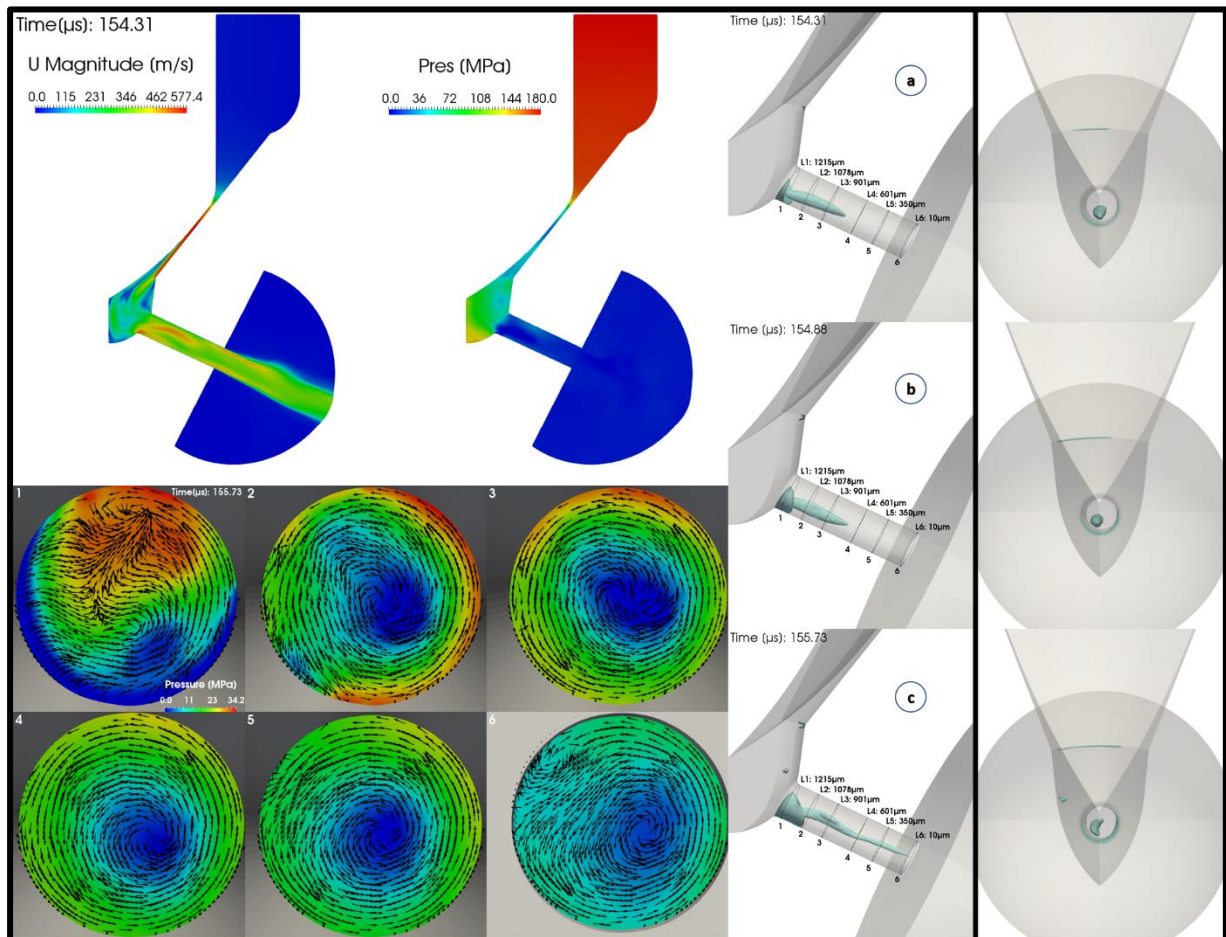
Figure 9. Left column: Velocity magnitude distribution at the midplane and Pressure distribution. Instantaneous pressure field and tangential vectors of velocity distribution on six cross-sections normal to the orifice of the injector. Right: Vapour distribution at three different instances (a-c). A series of images (a-c) illustrating the growth and the developed of the developed cavitation formation.

Conclusions

This paper assesses the potential of 2-phase cavitation model, coupled with the developed fully compressible density-based solver incorporating the transient effects of the injector geometry, in the prediction of erosion effects. A reliable prediction of erosion-sensitive areas due to collapse events during the opening of the needle could only be predicted accurately by including the unsteady needle motion with a fully compressible treatment of the liquid and the liquid-vapor mixture, resolving dynamics of shock waves. This numerical approach plays an essential role for the prediction of cavitation erosion and allows for the detection of erosion-relevant events. A high-frequency vortex cavitation, associated with boundary-layer separation and shear-layer instabilities at orifice and the needle seat passage, is the predominant cavitation mechanism. Moreover, there is very good correlation of the predicted potential erosion damage locations with the observed erosion patterns. Four different stages of the opening injection cycle have been defined, during which the flow characteristics differ significantly and determine the erosion pattern.

Disclaimer

Nomenclature

P	Density [kg/m^3]
U	Velocity field [m/s]
p	Pressure [Pa]
a_v	Vapour fraction
$\rho_{sat,L}$	Liquid density at saturation [kg/m^3]
$\rho_{sat,V}$	Vapour density at saturation [kg/m^3]
n	Tait equation exponent (for liquid)
p_{sat}	Saturation pressure [Pa]

Reference

[1] Örley, F., Hickel, S., Schmidt, S. J., and Adams, N. A., 2017, "Large-Eddy Simulation of Turbulent, Cavitating Fuel Flow inside a 9-Hole Diesel Injector Including Needle Movement," Int. J. Engine Res., **18**(3), pp. 195–211.

[2] Befrui, B., Corbinelli, G., Robart, D., Reckers, W., and Weller, H., 2008, *LES Simulation of the Internal Flow and Near-Field Spray Structure of an Outward-Opening GDi Injector and Comparison with Imaging Data*, 2008-01–0137, SAE International, Warrendale, PA.

[3] "High-Resolution Large Eddy Simulations of Cavitating Gasoline–Ethanol Blends - Daniel J Duke, David P Schmidt, Kshitij Neroorkar, Alan L Kastengren, Christopher F Powell, 2013" [Online]. Available: https://journals.sagepub.com/doi/abs/10.1177/1468087413501824. [Accessed: 18-Mar-2019].

[4] "Performance of Turbulence and Cavitation Models in Prediction of Incipient and Developed Cavitation - Phoevos Koukouvinis, Homa Naseri, Manolis Gavaises, 2017" [Online]. Available: https://journals.sagepub.com/doi/abs/10.1177/1468087416658604. [Accessed: 18-Mar-2019].

[5] Gavaises, M., Papoulias, D., Andriotis, A., Giannadakis, E., and Theodorakakos, A., 2007, *Link Between Cavitation Development and Erosion Damage in Diesel Injector Nozzles*, 2007-01–0246, SAE International, Warrendale, PA.

[6] Koukouvinis, P., Gavaises, M., Li, J., and Wang, L., 2016, "Large Eddy Simulation of Diesel Injector Including Cavitation Effects and Correlation to Erosion Damage," Fuel, **175**, pp. 26–39.

[7] Demirdžić, I., and Perić, M., 1988, "Space Conservation Law in Finite Volume Calculations of Fluid Flow," Int. J. Numer. Methods Fluids, **8**(9), pp. 1037–1050.

[8] Egerer, C. P., Hickel, S., Schmidt, S. J., and Adams, N. A., 2014, "Large-Eddy Simulation of Turbulent Cavitating Flow in a Micro Channel," Phys. Fluids, **26**(8), p. 085102.

[9] Ducros, F., Nicoud, F., and Poinsot, T., "Wall-Adapting Local Eddy-Viscosity Models for Simulations in Complex Geometries," p. 8.

[10] Dular, M., and Coutier-Delgosha, O., 2009, "Numerical Modelling of Cavitation Erosion," Int. J. Numer. Methods Fluids, **61**(12), pp. 1388–1410.

[11] "Mechanical Properties of Hardened AISI 52100 Steel in Hard Machining Processes | Journal of Manufacturing Science and Engineering | ASME DC" [Online]. Available: https://manufacturingscience.asmedigitalcollection.asme.org/article.aspx?articleid=1485018. [Accessed: 19-Mar-2019].

[12] "OpenFOAM 2.4.0," OpenFOAM [Online]. Available: https://openfoam.org/version/2-4-0/. [Accessed: 22-May-2019].

[13] Greenshields, C. J., Weller, H. G., Gasparini, L., and Reese, J. M., 2010, "Implementation of Semi-Discrete, Non-Staggered Central Schemes in a Colocated, Polyhedral, Finite Volume Framework, for High-Speed Viscous Flows," Int. J. Numer. Methods Fluids, **63**(1), pp. 1–21.

[14] Kurganov, A., and Tadmor, E., 2000, "New High-Resolution Central Schemes for Nonlinear Conservation Laws and Convection–Diffusion Equations," J. Comput. Phys., **160**(1), pp. 241–282.

[15] "Automatic-Mesh-Motion-for-the-Unstructured-Finite-Volume-Method.Pdf."

[16] Guillard, H., and Viozat, C., 1999, "On the Behaviour of Upwind Schemes in the Low Mach Number Limit," Comput. Fluids, **28**(1), pp. 63–86.

[17] Schmidt, S., Sezal, I., Schnerr, G., and Talhamer, M., "Riemann Techniques for the Simulation of Compressible Liquid Flows with Phase-Transistion at All Mach Numbers - Shock and Wave Dynamics in Cavitating 3-D Micro and Macro Systems," *46th AIAA Aerospace Sciences Meeting and Exhibit*, American Institute of Aeronautics and Astronautics.

[18] Kyriazis, N., Koukouvinis, P., and Gavaises, M., 2017, "Numerical Investigation of Bubble Dynamics Using Tabulated Data," Int. J. Multiph. Flow, **93**, pp. 158–177.

[19] Liou, M.-S., 2006, "A Sequel to AUSM, Part II: AUSM+-up for All Speeds," J. Comput. Phys., **214**(1), pp. 137–170.

[20] Toro, E. F., 2013, *Riemann Solvers and Numerical Methods for Fluid Dynamics: A Practical Introduction*, Springer Science & Business Media.

[21] Safarov, J., Ashurova, U., Ahmadov, B., Abdullayev, E., Shahverdiyev, A., and Hassel, E., 2018, "Thermophysical Properties of Diesel Fuel over a Wide Range of Temperatures and Pressures," Fuel, **216**, pp. 870–889.